Climatology of size, shape and intensity of precipitation features over Great Britain and Ireland

Article

CentAUR

Central Archive at the University of Reading

Reading's research outputs online

Climatology of Size, Shape, and Intensity of Precipitation Features over Great Britain and Ireland

JONATHAN G. FAIRMAN JR. AND DAVID M. SCHULTZ

Centre for Atmospheric Science, School of Earth and Environmental Sciences, University of Manchester, Manchester, United Kingdom

DANIEL J. KIRSHBAUM

Department of Atmospheric and Oceanic Sciences, McGill University, Montreal, Quebec, Canada

SUZANNE L. GRAY

Department of Meteorology, University of Reading, Reading, United Kingdom

ANDREW I. BARRETT

Institute of Meteorology and Climate Research, Karlsruhe Institute of Technology, Karlsruhe, Germany

ABSTRACT

A climatology of precipitation features (or objects) from the Great Britain and Ireland radar-derived precipitation mosaic from 2006 to 2015 is constructed, with features defined as contiguous areas of nonzero precipitation rates. Over the 10 years, there are 54 811 747 nonunique precipitating features over $100 \, \text{km}^2$ in area, with a median precipitation feature area of $249 \, \text{km}^2$, median major axis length of 29.2 km, median aspect ratio of 2.0:1, median feature mean precipitation rate of $0.49 \, \text{mm h}^{-1}$, and median feature maximum precipitation rate of $2.4 \, \text{mm h}^{-1}$. Small-scale precipitating systems are most common, but larger systems exceeding $10 \, 000 \, \text{km}^2$ contribute close to 70% of the annual precipitation across the study region. Precipitation feature characteristics are sensitive to changes in annual and diurnal environment, with feature intensities peaking during the afternoon in summer and the largest precipitation features occurring during winter. Precipitation intensities less than $5 \, \text{mm h}^{-1}$ comprise 97.3% of all precipitation occurrences and contribute 83.6% of the total precipitation over land. Banded precipitation features (defined as precipitation features with aspect ratio at least 3:1 and major axis length at least 100 km) comprise 3% of all precipitation features by occurrence, but contribute 23.7% of the total precipitation. Mesoscale banded features (defined as banded precipitation features with major axis length at least 100 km and total area not exceeding $10 \, 000 \, \text{km}^2$) and mesoscale convective banded features (defined as banded precipitation features with at least $100 \, \text{km}^2$ of precipitation rates exceeding $10 \, \text{mm h}^{-1}$) are most prevalent in southwestern England, with mesoscale convective banded features contributing up to 2% of precipitation.

1. Introduction

Surface precipitation is measured as the depth of liquid water (or liquid equivalent in the case of solid precipitation) observed at a point on the surface over a period of time. Because this single measurement of precipitation is sampling a precipitating system, such measurements cannot capture the size, shape, or maximum intensity of the system as a whole. Such characteristics can, however, be determined from automated feature-based (also called object based) analysis of two-dimensional precipitation fields.

Corresponding author: Dr. Jonathan G. Fairman, jonathan.fairman@manchester.ac.uk

Automated precipitation climatologies have typically focused on information from satellites, with data from the Tropical Rainfall Measuring Mission (TRMM; Kummerow et al. 1998) being the most prevalent. TRMM is composed of two instruments, the Precipitation Radar and TRMM Microwave Imager. The TRMM Precipitation Radar only provides a relatively small swath, so some regions may only be sampled on average every few days, although sampling is improved using the TRMM Microwave Imager. For example, TRMM data from the PR 2A-25 reflectivity dataset in combination with the 85-GHz polarization-corrected temperatures from the TRMM Microwave Imager forms the backbone of the University of Utah TRMM precipitation feature database (Nesbitt et al. 2000). This precipitation feature database has been explored for global distribution of storms with lighting (Cecil et al. 2005), extreme thunderstorms (Zipser et al. 2006), and convective features within tropical cyclones (Jiang et al. 2011). Liu et al. (2008) extended this database to include information about feature size. TRMM data have also been used to develop climatologies of different geographic regions and for analyses of storm characteristics (Liu and Zipser 2013; Rapp et al. 2014; Xu and Rutledge 2015; Rasmussen et al. 2016). Because the TRMM Precipitation Radar only collects data from 37.5°S to 37.5°N and only samples a given area once every few hours, short-lived precipitation features in the tropics and all precipitation features in the midlatitudes are excluded from these studies. The Global Precipitation Measurement mission (Hou et al. 2014; Skofronick-Jackson et al. 2017) does cover Great Britain and Ireland, but there are no feature-based climatologies yet from this dataset. Other precipitation feature analyses have used data from the W-band radar on board *CloudSat* (e.g., Smalley and L'Ecuyer 2015), but TRMM provides a narrow swath of data, whereas *CloudSat* only provides a subsatellite track. As a result, continuous data collection over small regions is simply not yet possible from satelliteborne radars.

Land-based radars over the United States have been used for feature-based identification of precipitation features. Rickenbach et al. (2015) used the National Mosaic and Multi-Sensor Quantitative Precipitation Estimation (NMQ) dataset of Zhang et al. (2011) to determine the effect of mesoscale precipitation features on annual and diurnal precipitation accumulations in the southeastern United States over a 4-yr period, finding that over 70% of precipitation originated from mesoscale precipitation features across much of the domain. Fairman et al. (2016) used an automated feature-based detection algorithm to determine the climatology of banded precipitation across the contiguous United States using 5-min NEXRAD mosaics, finding that precipitation coverage was the largest during the

afternoon hours from April to August and that a large difference in the proportion of banded precipitation existed on the east and west sides of the Rockies. Finally, Kirshbaum et al. (2016) used the NEXRAD composites to study the climatological occurrence of deep convection over the southern Mississippi Valley, finding that afternoon convection inside the valley was suppressed during the summer months. Note that the NEXRAD [Multi-Radar/Multi-Sensor (MRMS)] composite is on a 0.01° and 2-min resolution versus the resolution of 1 km and 5 min over Great Britain and Ireland. These recent studies show the value of using land-based radar mosaics to determine the distribution of precipitation feature characteristics and their contribution to climatology. Although there are numerous issues in the use of radar data for climatological studies (such as artifacts within the data), ground-based radar provides the only effective means of obtaining continuous large-scale instantaneous spatial measurements of precipitation.

Over Great Britain and Ireland, the radar-derived precipitation mosaic (Met Office 2009) provides a reasonably accurate spatial representation of precipitation accumulation on multiyear time scales (Fairman et al. 2015) and can be used to calculate two-dimensional data of precipitation feature area, shape, and intensity. This present study uses the radar precipitation mosaic over Great Britain and Ireland to classify all precipitating storms at 5-min intervals from 2006 to 2015, providing a decade of analysis of the characteristics of precipitating features. These feature characteristics are then analyzed in time and space across the radar mosaic coverage area. This study uses similar methods to those of Fairman et al. (2016), but uses the precipitation rate retrieval by the Met Office radar-derived precipitation mosaic rather than the radar reflectivities in the NEXRAD composites. The individual impacts of precipitation feature size, intensity, and shape on precipitation accumulation are all considered in turn. The climatology that can be formed from this feature database can serve as a check on the output from numerical forecast models to verify precipitation morphology is forecast correctly. It can also be used to search for individual morphologies of precipitation features, such as precipitation bands, as Fairman et al. (2016) did for the contiguous United States. It can also be used to link precipitation morphologies with synoptic figures identified independently, for example, from reanalyses. Such an approach could improve the understanding of larger-scale dynamical influences on precipitation structures.

The rest of this paper is structured as follows. Section 2 of this paper describes the two-dimensional radar-derived precipitation mosaic and the precipitation feature detection algorithm. Section 3 presents the climatology of the precipitation features and cumulative distribution of

some relevant precipitation feature characteristics. The diurnal and annual cycles of these precipitation feature characteristics are described in section 4. Section 5 presents the spatial distribution of radar-derived precipitation rates, whereas section 6 discusses the spatial distribution of the occurrence and contribution to the total precipitation of precipitation features of different areas. Section 7 contains the occurrence of banded precipitation features, mesoscale banded features, and mesoscale convective banded features, which are obtained by setting thresholds on feature size, shape, and intensity. Section 8 is a discussion of the results compared to other feature-based studies over the United States and around the world, and section 9 concludes this article.

2. Data and methods

This study uses the Met Office radar-derived precipitation mosaic (Met Office 2003, 2009) to identify individual precipitation features from 2006 to 2015. This dataset has been generated at 1-km grid spacing at 1-km constant-altitude plan position indicator (CAPPI) since 2006 and is derived from a mosaic analysis of radar reflectivity from the radar networks of the United Kingdom and the Republic of Ireland (Kitchen and Illingworth 2011). Figure 1 shows the Great Britain and Ireland radar network and the 18 radar sites that comprise it. Of these 18 radar sites, 16 are operated by the Met Office, with 14 on the island of Great Britain, one in Northern Ireland, and one on the island of Jersey. The Irish National Meteorological Service (Met Éirrean) operates the two radars in the Republic of Ireland (Shannon and Dublin). Since 2005, the radar mosaic has been processed under the data processing chain described by Harrison et al. (2009). Not all of the radars provide continuous data, with several having intermittent outages. This is particularly evident at the radar at Shannon, which operated on a 15-min frequency during much of the study period.

The Great Britain and Ireland radar network is composed of C-band (5.6-m wavelength) radars, which measure radar reflectivity factor at 5-min intervals. These data are then converted from radar reflectivity Z to a precipitation rate R by a constant Z–R power law relationship of $Z = 200R^{1.6}$ (Marshall and Palmer 1948; Marshall et al. 1955). Because this retrieval assumes that all droplets are liquid, the radar reflectivity is thus expressed as an equivalent rain rate, regardless of the actual type of precipitation at the surface. This rain rate is then corrected for orographic variation (Georgiou et al. 2011) and adjusted for consistency with nearby gauge information on a radar-by-radar basis (Kitchen et al. 1994; Lewis and Harrison 2007; Harrison et al. 2012). This adjustment is based on long-term relationships between
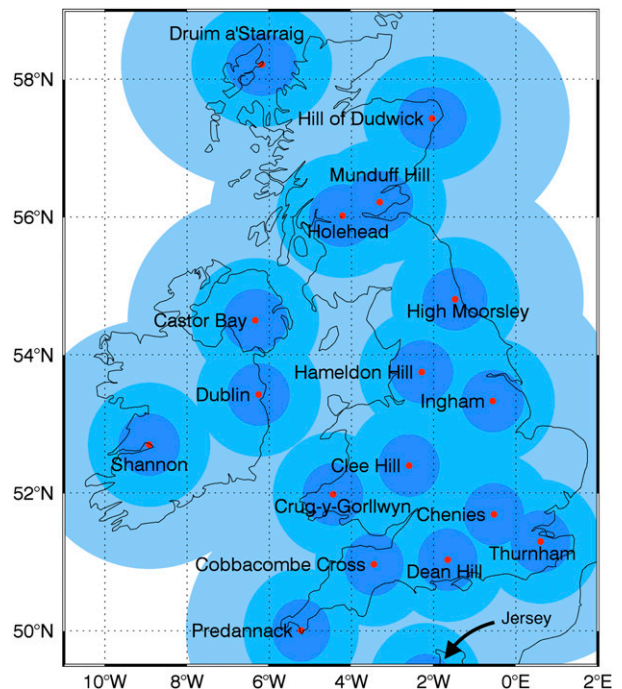

FIG. 1. Locations of Met Office and Met Éirrean radar sites (labeled red dots) comprising the Met Office 1-km radar-derived precipitation composite. The filled circles indicate distances of 50, 100, and 200 km from the individual radars.

the radar-derived precipitation rate and gauge measurements in each radar catchment area. These retrieved precipitation rates are then mosaicked to a uniform grid, with the individual observations weighted by both distance to the radar and pixel quality (Harrison et al. 2009). Further information about the data processing is provided in section 3a of Antonescu et al. (2013). Fairman et al. (2015) showed that the difference of annual average precipitation from the radar mosaic over Great Britain and Ireland compared to gauge values was $+29\,\mathrm{mm\,yr^{-1}}$, within 3% of the annual average gauge total. An example radar image at 1200 UTC 9 July 2012 is shown in Fig. 2a.

To determine the influence of shape, size, and intensity of individual storms on Great Britain and Ireland precipitation, each radar image is processed to determine individual precipitation features. In this study, a precipitation feature is defined as a contiguous area greater than or equal to $100\,\mathrm{km^2}$ with a nonzero precipitation rate, with contiguity being defined as a connection in any direction to another precipitating point. The threshold of $100\,\mathrm{km^2}$ was chosen to limit influence of small-scale radar effects and clutter that may not be precipitating systems. All feature area calculations were performed on the original dataset (1 km $\times$ 1 km for each pixel) without any alterations in the map projection. This process detects 54 811 747 features over the 10 years of
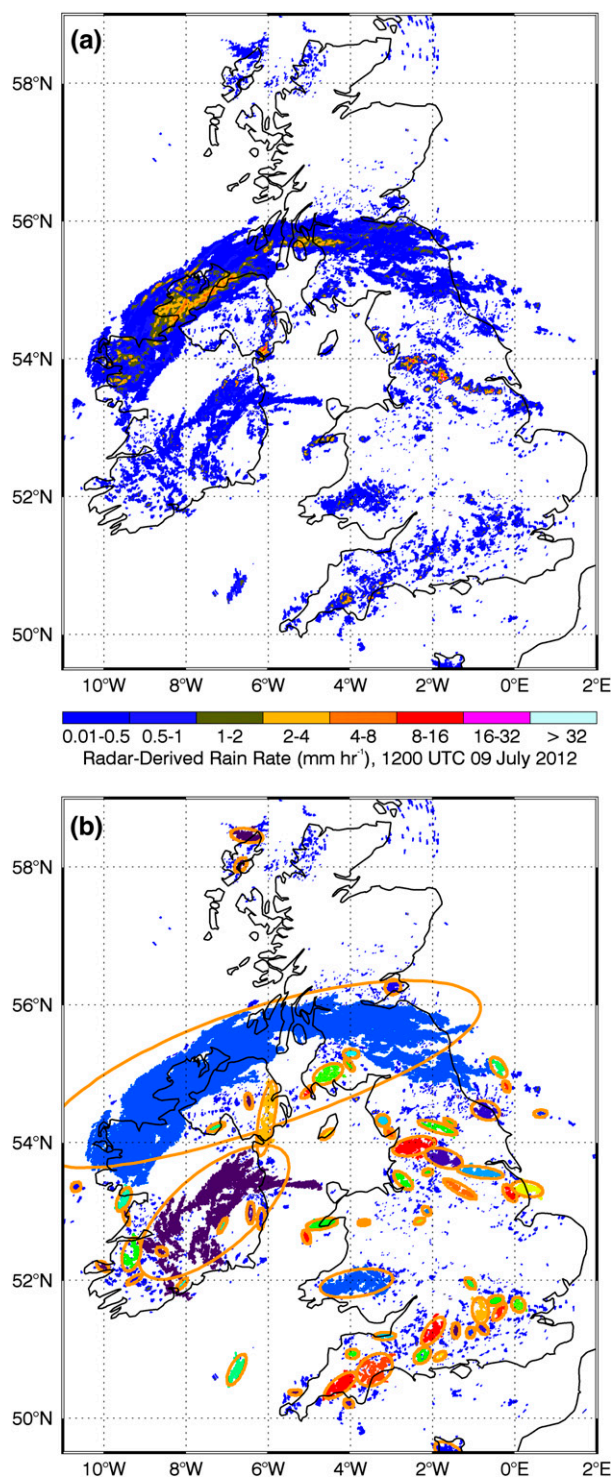
FIG. 2. (a) Example of radar-derived rain rate (colored according to scale) at 1200 UTC 9 Jul 2012. (b) Fitted ellipses and detected precipitation features at 1200 UTC 9 Jul 2012, with each color indicating a separate feature.

data. Note that these features are not necessarily unique, as an individual precipitating storm will most likely span multiple time steps. To determine major and minor axis lengths of the individual precipitation features, a mass-density method of ellipse fitting was used (see appendix for details). The mass-density approach of ellipse fitting has been used in other feature-detection studies (e.g., Nesbitt et al. 2006; Xu et al. 2015; Fairman et al. 2016) and is illustrated on an example image in Fig. 2b.

Although the radar network over Great Britain and Ireland is fairly contiguous, there are still some potential coverage gaps over the Irish Sea and other areas that are farther than 100 km from a radar site. The farthest distances are shown as the lightest shade of blue in Fig. 1. These gaps can disrupt feature detection, as can the extension of precipitation features beyond the boundaries of the radar composite. Additionally, no alterations to the base data are made to remove any nonphysical radar-based artifacts, which may influence the results from this analysis. These nonphysical radar-based artifacts may include gaps in coverage along some azimuths that could lead to errors in the spatial distribution of feature size, with a bias toward smaller and more banded features in the areas of spokes.

The precipitation features are then classified by their shape, size, and intensity. Different thresholds are used to determine specific types of precipitation features. In this study, a banded precipitation feature is defined as a precipitation feature having an aspect ratio (defined as the ratio between the major and minor axes of the fitted ellipse) greater than or equal to 3:1 and a major axis length greater than or equal to 100 km. This definition is the same as used in Fairman et al. (2016), but differs from the more stringent 5:1 aspect ratio defined by Liu and Zipser (2013). A mesoscale banded precipitation feature is a banded precipitation feature with a major axis length greater than or equal to 100 km and a total area not exceeding $10\,000\,\mathrm{km}^2$. A mesoscale convective banded precipitation feature has the same requirements as a mesoscale banded precipitation feature, but also requires at least $100\,\mathrm{km}^2$ of the feature to exhibit precipitation rates exceeding $10\,\mathrm{mm}\,\mathrm{h}^{-1}$. These mesoscale convective bands are smaller than a squall line or mesoscale convective complex as defined by Maddox (1980) by at least an order of magnitude. Of the 54 811 747 precipitation features detected herein, 1 803 029 (3.2%) are banded features, 1 423 485 (2.5%) are mesoscale banded features, and 50 474 (0.09%) are mesoscale convective banded features.

Two factors are considered to evaluate the effects of size, shape, and intensity of precipitation features on the precipitation climatology of the study region: the hours per year that precipitation features possess these
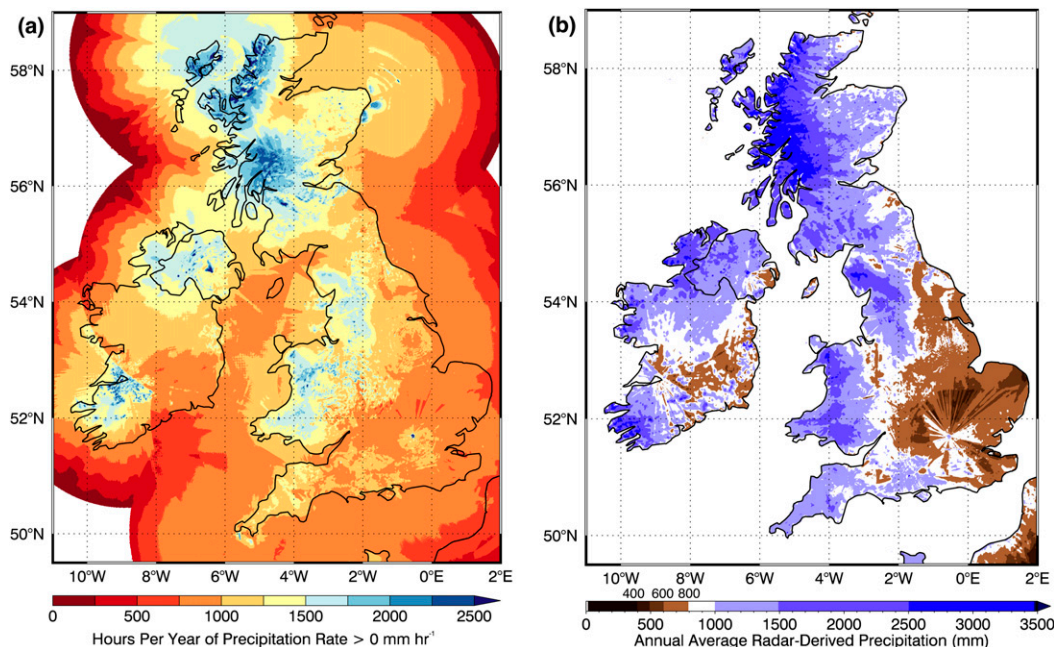
FIG. 3. (a) Hours per year of precipitation rate exceeding $0 \, \mathrm{mm \, h^{-1}}$ from 2006 to 2015 ($\mathrm{mm \, h^{-1}}$; colored according to scale). (b) Annual average precipitation over land from 2006 to 2015 (mm; colored according to scale).

characteristics (defined as occurrence) and the percentage contribution of these features to the annual total precipitation. These complementary metrics allow comparison of the hours per year when the precipitation occurs (Fig. 3a) and annual average precipitation (Fig. 3b). Precipitation totals in Fig. 3b and thereafter are not shown over the ocean as the retrieval algorithm is only verified over land (Harrison et al. 2012; Fairman et al. 2015). Nonetheless, the algorithm uses the full radar composite area to determine feature characteristics as to not introduce spurious gaps.

The annual radar-derived precipitation mosaic over Great Britain and Ireland shows an annual precipitation occurrence maximum exceeding $2500 \, \mathrm{h \, yr^{-1}}$ (28.5%, Fig. 3a) over the west coast of Scotland. Other areas of high precipitation occurrence (over $1500 \, \mathrm{h \, yr^{-1}}$ or 17.1%) include Northern Ireland, northwestern England, and the majority of Wales. Not surprisingly, these areas are typically where the highest precipitation accumulations occur (Fig. 3b), with over $3000 \, \mathrm{mm \, yr^{-1}}$ over the west coast of Scotland. However, in both the occurrence and precipitation totals there is a large east–west gradient, with eastern England receiving less than $800 \, \mathrm{mm \, yr^{-1}}$ of precipitation from less than $1000 \, \mathrm{h \, yr^{-1}}$ (11.4%) of precipitation. A discontinuity in both the precipitation occurrence and precipitation totals near the Shannon radar in southwestern Ireland is due to the intermittent operation of this radar over the study period. There are also noticeable radar lobes off the east

coast of Scotland (apparent at 57°N, 2°W) that may influence feature detection over the ocean in this region. These lobes may be due to mapping anomalies from the original radial radar data to the 2D composite grid. Finally, the regions surrounding the Chenies radar near London have beam-based artifacts due to surface clutter that appear both in the precipitation occurrence and precipitation total and that may cause gaps in precipitation features in this area. On average over the radar coverage area (defined as the outer boundary of the overlapping 200-km-range rings in Fig. 1), there are $822 \, \mathrm{h \, yr^{-1}}$ (9.4%) of precipitation occurrence that result in a mean annual total of 788 mm of precipitation.

3. Great Britain and Ireland precipitation feature characteristics

Five characteristics are used to determine the size, shape, and intensity of the precipitation features detected from the Great Britain and Ireland radar mosaic: horizontal area, length of the major axis, aspect ratio (the ratio of the lengths of the major and minor axes), maximum rain rate within the feature, and mean rain rate of the feature. The feature area has a lognormal distribution, with 85% of all features smaller than $1000 \, \mathrm{km^2}$ and 95% of all features smaller than $3000 \, \mathrm{km^2}$ in area (Figs. 4a,b). The largest detected precipitation feature ($670\,797 \, \mathrm{km^2}$ in area) occurred at 2100 UTC 5 March 2007, when a long precipitating front extended
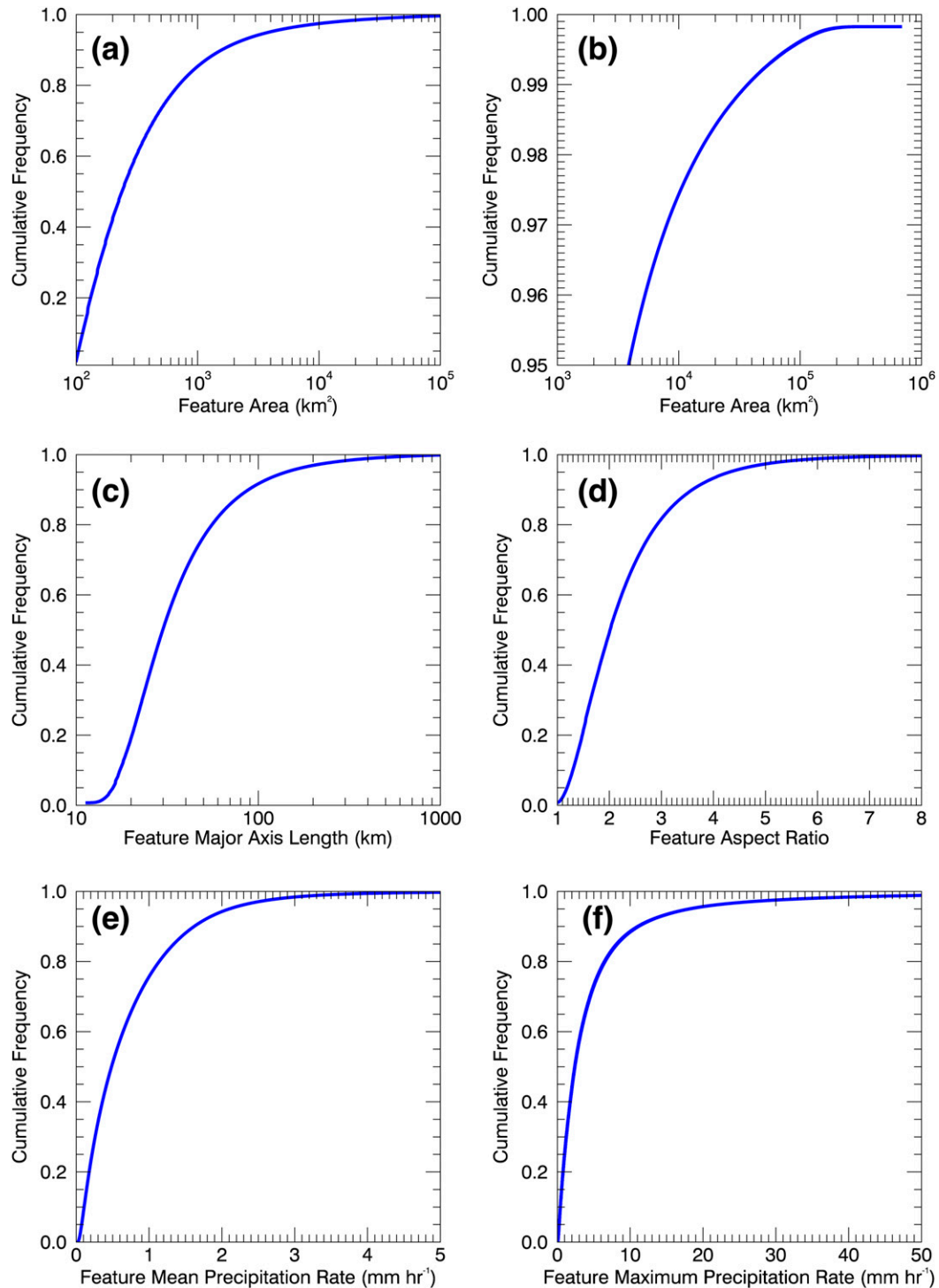
FIG. 4. Cumulative frequency diagrams of precipitation feature characteristics for the dataset used in this study: (a) area, (b) area from 95% to 100%, (c) major axis length, (d) aspect ratio, (e) mean precipitation rate, and (f) maximum precipitation rate.

across nearly the entire west coast of Great Britain and over much of the Irish Sea. Only 0.038% (210 325) of all precipitation features exceed $100\,000\,km^2$ in area. For context, the total study area comprises $3\,751\,875\,km^2$, meaning that a feature of $100\,000\,km^2$ comprises 2.6% of the study area. The mean and median feature sizes are 1927 and $239\,km^2$, respectively.

The distribution of feature major axis length is slightly different than that of feature size (cf. Figs. 4a,c) but is lognormal for major axis lengths exceeding 15 km, which is reasonable considering that the diameter of a perfectly circular $100\,km^2$ feature is 11.3 km and the minimum major axis in the database is 11.4 km. Over 90% of precipitation features have major axis lengths less than 100 km, and only 0.1% of all precipitation features have major axes exceeding 1000 km. The longest major axis of any precipitation feature was 1860 km and occurred at 2035 UTC 3 June 2007 when a squall line existed across much of Great Britain. The mean major axis length is 51.7 km, exceeding the median value of 29.9 km.

The distribution of aspect ratio (Fig. 4d) shows a similar pattern to major axis length. The highest aspect ratio of 66.9:1 occurred at 2315 UTC 21 June 2010, caused by spurious radar features over the Irish Sea in the domain of the Shannon radar. Only 2.7% (1 467 826) of all features have an aspect ratio higher than 5:1. The mean feature aspect ratio is 2.3:1, with the median being 2.0:1, indicating that most precipitation features across Great Britain and Ireland are not particularly elongated.

Because the radar mosaic provides precipitation rates, the mean (Fig. 4e) and maximum precipitation rate (Fig. 4f) over each feature can be determined. Both of these characteristics follow a similar lognormal distribution to the rest of the precipitation feature characteristics. In general, the mean precipitation rate is less than $1\,mm\,h^{-1}$, with only 24.6% (13 522 572) of all precipitation features exceeding this value and only 5.8% (3 202 810) exceeding $2\,mm\,h^{-1}$. The average of all feature mean precipitation rates is $0.73\,mm\,h^{-1}$, with the median being $0.49\,mm\,h^{-1}$. Only 0.25% (135 858) of all precipitation features have a mean rainfall rate exceeding $5\,mm\,h^{-1}$, with the highest value of mean precipitation rate of $107\,mm\,h^{-1}$ associated with a persistent radar processing error that occurred near the Castor Bay radar in Northern Ireland at 0640 UTC 29 September 2008.

The cumulative frequency of the maximum precipitation rate (Fig. 4f) follows a similar pattern to the other precipitation feature characteristics, but has a steeper initial slope compared to the mean precipitation rate (Fig. 4e). Whereas 75.3% (41 418 461) of all precipitation features have a maximum precipitation rate exceeding $1\,mm\,h^{-1}$, only 56.5% (30 982 046) of all precipitation features have maximum rain rates exceeding

$2\,mm\,h^{-1}$, meaning that 43.5% of all precipitation features in the United Kingdom would be classified as "slight showery rain" (Met Office 1997). Only 11.5% (6 327 379) of all precipitation features have a maximum precipitation rate exceeding $10\,mm\,h^{-1}$, a threshold that others have used to identify convection (Leary and Houze 1979; Xu et al. 2014) and the upper limit of moderate showery precipitation as classified by the Met Office. Few (3.2%, 1 746 302) precipitation features have maximum rainfall rates exceeding $25\,mm\,h^{-1}$. Only identifying features exceeding $100\,km^2$ may lead to small convective features being missed. However, proportionally few (5%) features with precipitation rates exceeding $25\,mm\,h^{-1}$ fall within $100-150\,km^2$ compared to 25% of all precipitation features. There are multiple occurrences of unphysical rain rates (those exceeding $128\,mm\,h^{-1}$), which comprise 0.14% (77 087) of the maximum precipitation rate of all precipitation features and may be associated with hail or other misidentification by the Met Office retrieval algorithm. No efforts were made to remove unphysical retrievals in study as overall they occur with such small frequency as to have little effect on the mean and median statistics. The mean and median maximum precipitation rates are 5.29 and $2.40\,mm\,h^{-1}$, respectively.

4. Diurnal and annual cycles in shape, size, and intensity

Analysis of the diurnal patterns over the entire year shows the effects of seasonal weather pattern shifts and daily meteorological cycles (Fig. 5). Figure 5 was created through averaging precipitation feature data in 10-day and hourly increments to form a 37×24 array. There is much more total precipitation area from the middle of September through early February over the study region, although the diurnal variation is small (Fig. 5a). In late September, the total precipitation area increases abruptly from below $0.7 \times 10^5\,km^2$ to over $1 \times 10^5\,km^2$, most likely related to a strengthening and eastward movement of the jet stream from the center of the Atlantic to the U.K. region (Woollings et al. 2014; N. Ridding 2014, personal communication). During late October, early November, and mid-January, precipitation covers the most area in the overnight hours, particularly from 0200 to 0500 UTC in late October and mid-January.

The largest values of mean feature area occur overnight (2300–0900 UTC) during January (Fig. 5b). However, similar values of mean feature area are present overnight over much of the first half of the year, outside of a few weeks in late March and early April. Such discontinuities in the annual precipitation cycle likely relate to the relatively short period of the climatology. Although the total precipitation area increases in
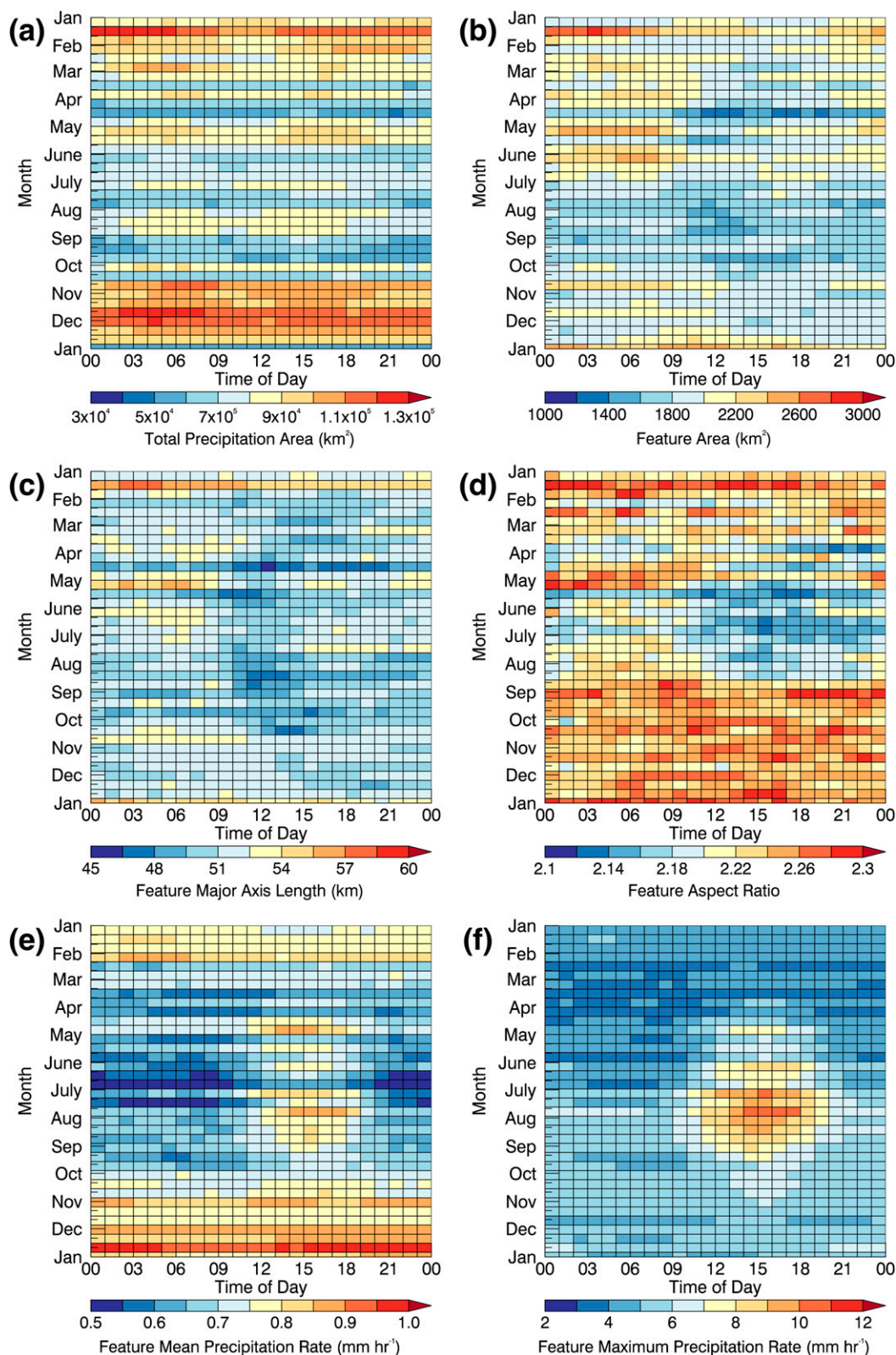
FIG. 5. Diurnal cycles over the year of precipitation feature characteristics (time; UTC): (a) total area covered by precipitation, (b) precipitation feature area, (c) precipitation feature major axis length, (d) precipitation feature aspect ratio, (e) precipitation feature mean precipitation rate, and (f) precipitation feature maximum precipitation rate.

the autumn, the feature size does not, indicating that the increase in total precipitation area is due to an increase in the number of features. The variations in feature major axis length (Fig. 5c) are broadly similar to those in mean feature area, showing the same overnight peaks during the first half of the year and midday minima during the summer. The annual variation in aspect ratio (Fig. 5d) shows that features tend to be slightly more elongated (larger aspect ratios) from August through January and more circular (smaller aspect ratios) during the afternoons from May through July.

The variations in mean precipitation rate (Fig. 5e) and maximum precipitation rate (Fig. 5f) exhibit some notable differences. The former (Fig. 5e) shows maximum values of about $1 \, \mathrm{mm \, h^{-1}}$ from October through December, with relatively large values extending into February. The lowest values occur overnight in June and July, when the mean precipitation rate falls below $0.5 \, \mathrm{mm \, h^{-1}}$. Whereas there is little diurnal variation in mean precipitation rate during the cool season, a strong diurnal cycle is found during the summer months, with a clear afternoon increase from April through August. This afternoon increase coincides with the increase in the maximum precipitation rate (Fig. 5f), with peak values occurring at around 1500 UTC, likely due to developing and/or strengthening convective cells. As for the mean precipitation rate, there is little diurnal variation in the maximum precipitation rate outside of the warm season. Therefore, the increase in the mean precipitation rate in winter is due to more moderate stratiform precipitation.

The diurnal patterns over the course of the year do grossly simplify the patterns of rainfall across Great Britain, as precipitation often will align with the Scottish Highlands and over the Pennines in the center of northern England. Topographic alignment may be a reason why there is a clear diurnal and annual signal in precipitation rate, but there is not a similar change in terms of the precipitation aspect ratio or feature size.

5. Intensity of Great Britain and Ireland radar-derived precipitation

Precipitation intensity is directly tied to the amount of precipitation accumulation over the course of the year. Several factors such as topographic complexity and the proximity to the ocean affect the magnitude and frequency of precipitation rates and their total contribution to the annual precipitation (Fairman et al. 2015). Quantification of the spatial patterns in precipitation feature intensity will also facilitate comparison with the spatial pattern in feature characteristics discussed in sections 6 and 7. We consider four bins of precipitation

intensity: 0–1, 1–5, 5–10, and >10 $\mathrm{mm \, h^{-1}}$ (Fig. 6). These bins of precipitation intensity are roughly comparable to "slight showery rain," "moderate showery rain," "moderate showery rain," and "heavy rain" by the *Forecasters' Reference Book* (Met Office 1997).

Precipitation rates of 0–1 $\mathrm{mm \, h^{-1}}$ (Fig. 6a) are the most frequent over Great Britain and Ireland, with up to 1500 $\mathrm{h \, yr^{-1}}$ (17.1%) of light precipitation over the west coast of Scotland and in the center of England and Wales. There is an average of 583 $\mathrm{h \, yr^{-1}}$ (6.6%) of precipitation from 0 to 1 $\mathrm{mm \, h^{-1}}$ across the study area. Several of the aforementioned radar-based artifacts are apparent for this intensity bin, especially near Shannon, Castor Bay, and Druim a'Starraig. The central half of Ireland is also very inconsistent compared to the north and southeast. There is a weak east–west gradient across most of northern England for this bin, showing that light rain is slightly more common over Ireland and western Great Britain.

A much smoother map is obtained for larger rain rates of 1–5 $\mathrm{mm \, h^{-1}}$ (Fig. 6b). This bin exhibits the highest occurrence on the west coast of Scotland, where values exceed 1050 $\mathrm{h \, yr^{-1}}$ (11.9%). There are also local maxima over the Lake District, Wales, Cornwall, and the northwest coast of Ireland with over 450 $\mathrm{h \, yr^{-1}}$ (5.1%) of occurrence. The average occurrence of precipitation rates from 1 to 5 $\mathrm{mm \, h^{-1}}$ over the radar coverage area is 222 $\mathrm{h \, yr^{-1}}$ (2.5%).

The occurrences of precipitation rates in the two bins exceeding 5 $\mathrm{mm \, h^{-1}}$ (Figs. 6c,d) have very similar distributions, and these rates are generally less frequent than the smaller rates. The areas with the most frequent occurrence of higher precipitation rates are the west coast of Scotland, where the average annual occurrence of precipitation rates between 5 and 10 $\mathrm{mm \, h^{-1}}$ can exceed 150 $\mathrm{h \, yr^{-1}}$ (1.7%) and the average annual occurrence of precipitation rates exceeding 10 $\mathrm{mm \, h^{-1}}$ can exceed 25 $\mathrm{h \, yr^{-1}}$ (0.3%). On average, there are 14.4 $\mathrm{h \, yr^{-1}}$ (0.2%) of precipitation rates from 5 to 10 $\mathrm{mm \, h^{-1}}$ across the study region and 2.7 $\mathrm{h \, yr^{-1}}$ (0.03%) of precipitation rates exceeding 10 $\mathrm{mm \, h^{-1}}$. Individual topographic features strongly impact these distributions, such as the Welsh Hills, the Lake District, and the Peak District.

Compared to the occurrence of different precipitation rates, the contribution of these rates to the overall precipitation is much more uniform. Precipitation rates of 0–1 $\mathrm{mm \, h^{-1}}$ (Fig. 7a) contribute only around half that of precipitation rates from 1 to 5 $\mathrm{mm \, h^{-1}}$ (Fig. 7b), with average values of 27% and 56%, respectively. Areas of high elevation or topographic variation generally have less contribution from precipitation rates from 0 to 1 $\mathrm{mm \, h^{-1}}$, with less than 7.5% of the precipitation total
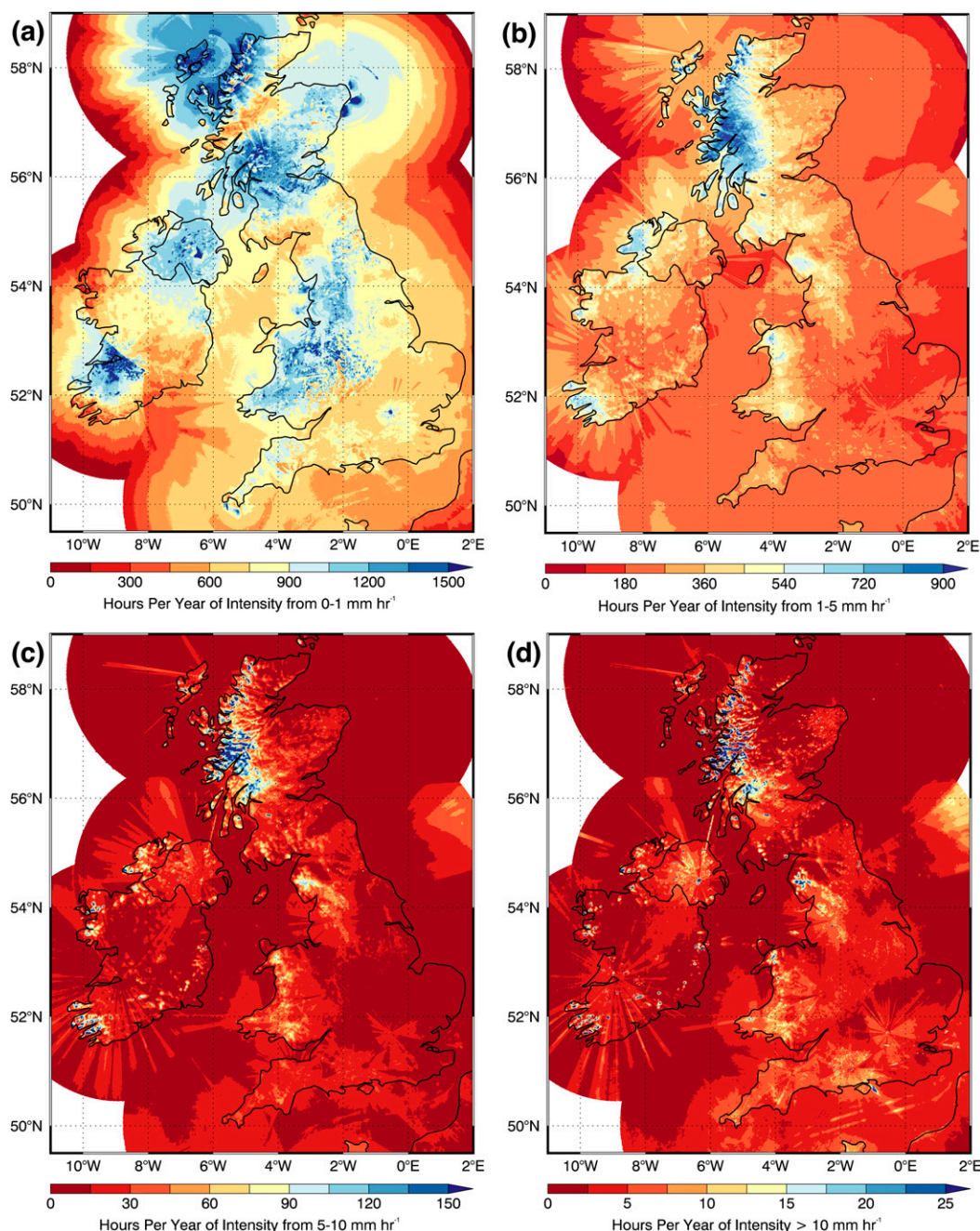
FIG. 6. Hours per year of occurrence of precipitation intensity for different intensity bins: (a) 0–1, (b) 1–5, (c) 5–10, and (d) exceeding $10\,\mathrm{mm\,h^{-1}}$. Note that scales vary.

in the west coast of Scotland and less than 15% of rainfall over the center of the Lake District.

Precipitation rates from 5 to $10\,\mathrm{mm\,h^{-1}}$ (Fig. 7c) have the most spatial variation out of all four bins. In most areas, less than 10% of the annual precipitation total comes from precipitation rates in this range. Over the areas of complex terrain such as Cornwall, Wales, the Lake District, and the west coast of Scotland, these rates

contribute up to 25% of the annual total. On average, precipitation rates from 5 to $10\,\mathrm{mm\,h^{-1}}$ contribute 11.1% of the annual rainfall total, which decreases further to 5.3% for rainfall rates exceeding $10\,\mathrm{mm\,h^{-1}}$ (Fig. 7d). These highest precipitation rates contribute the most to precipitation in the southern parts of Great Britain, along with isolated areas near the west coast of Scotland. Because these features are relative, fewer light rain events
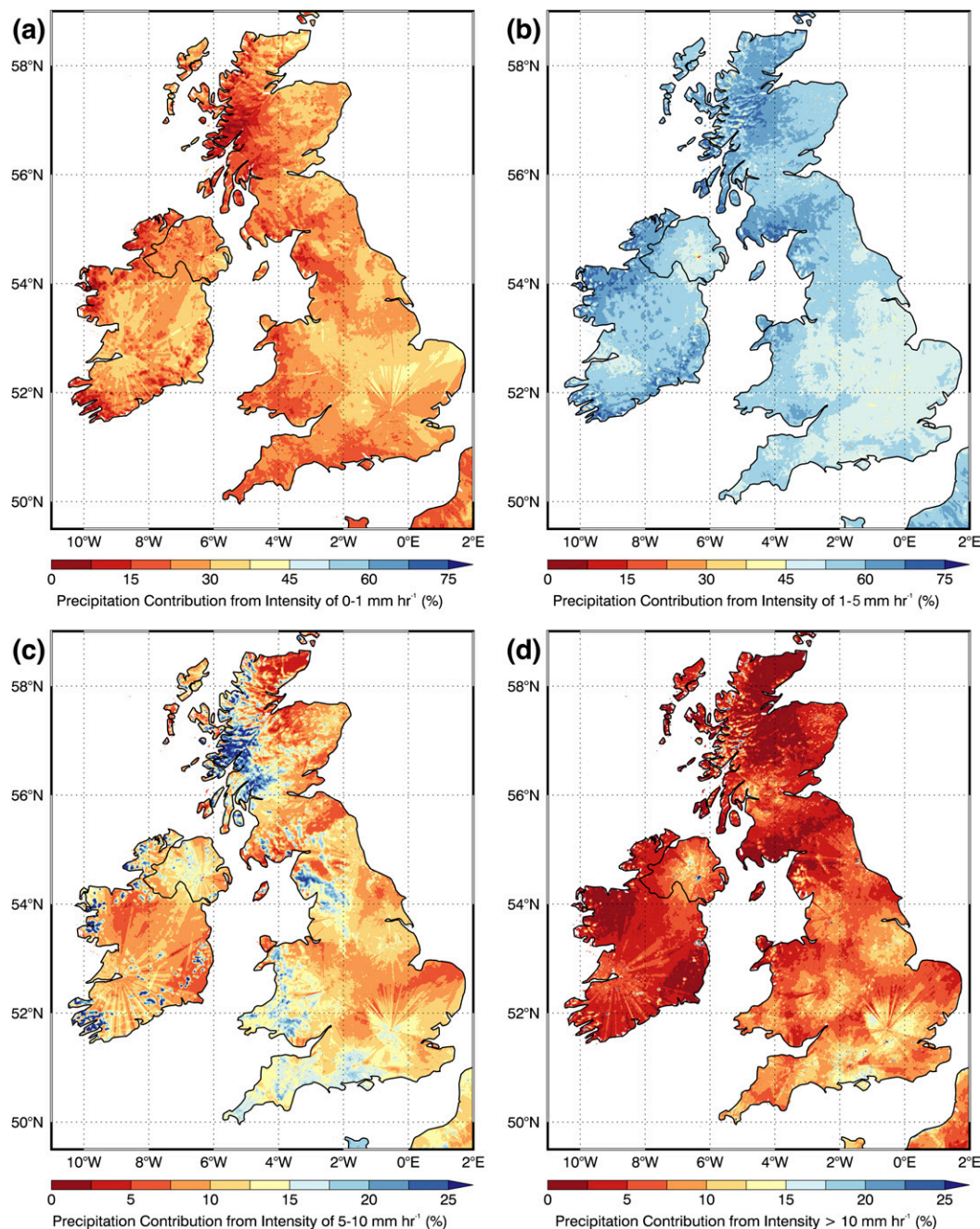
FIG. 7. Contribution to the annual precipitation total (%) from different precipitation intensity bins: (a) 0–1, (b) 1–5, (c) 5–10, and (d) exceeding 10 mm h^{-1}. Note that scales vary.

(compared to moderate and heavy intensity events) may be detected in southern England due to these events being in close proximity to the Chenies radar.

6. Size of the precipitation features

Precipitation feature size is separated into five bins: less than 100, 100–1000, 1000–10 000, 10 000–100 000, and 100 000 km^2 or greater. Note that the characteristics of features less than 100 km^2 in size are not included in the previous analysis. Characteristic sizes of these bins in relation to the study area are shown in Fig. 8, and the spatial patterns of occurrence of each of these feature size bins are shown in Fig. 9.

Although small features are omitted from the precipitation feature database, their relative spatial effect
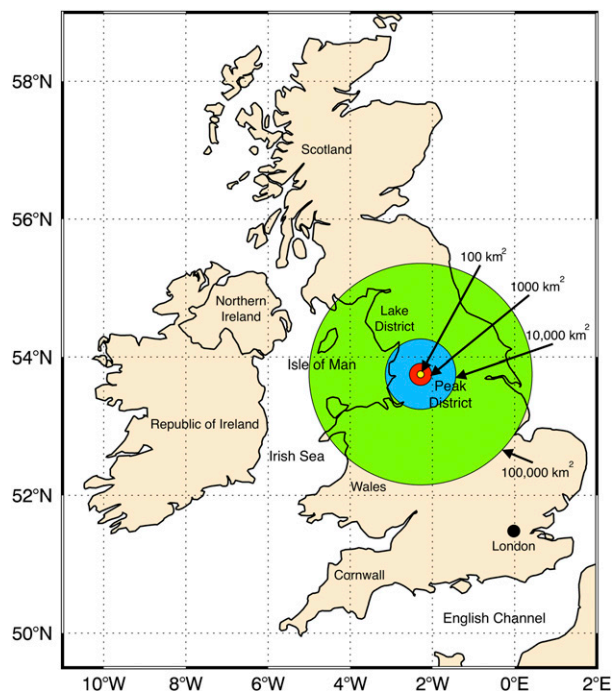
FIG. 8. Representative sizes of precipitation features (aspect ratio of 1.0:1) used for size bins in this study, centered on the location of the Hameldon Hill radar near Manchester. Yellow indicates a precipitation feature with an area of $100 \, \mathrm{km}^2$, red indicates $1000 \, \mathrm{km}^2$, blue indicates $10\,000 \, \mathrm{km}^2$, and green indicates $100\,000 \, \mathrm{km}^2$.

on precipitation occurrence can still be determined (Fig. 9a). There are small significant maxima potentially due to convection in southern Great Britain and western Wales. There may also be a maximum in storm occurrence east of London (coinciding with the Chenies radar) due to the urban heat island effect. However, most of the detected precipitation features that are less than $100 \, \mathrm{km}^2$ can be related to ground clutter near radars, topography, or in coastal locations. On average, these features are present for $58.6 \, \mathrm{h \, yr^{-1}}$ (0.7%) over Great Britain and Ireland. Maxima are apparent around most of the radar locations in Fig. 1. The highest values of occurrence of features less than $100 \, \mathrm{km}^2$ (exceeding $400 \, \mathrm{h \, yr^{-1}}$, 4.6%) are found on the northwest coast of Scotland (57°–58°N, 4°–6°W) and over much of central Scotland between Glasgow and Edinburgh (55°–57°N, 2°–5°W), near the Shannon radar in Ireland (52.5°N, 9°W), and the West Midlands in England and eastern Wales (52°–53°N, 2°–4°W).

For larger precipitation feature areas of 100–$1000 \, \mathrm{km}^2$, much of the apparent clutter is reduced, but probably not eliminated entirely (Fig. 9b). The spatially averaged time of occurrence is $95.6 \, \mathrm{h \, yr^{-1}}$ (1.1%). These smaller-scale precipitation features tend to occur in areas such as the complex topography in Cornwall near 51°N, 4°W,

most of Wales (52°–53°N, 3°–5°W), and the Pennines and center of the Lake District (54.5°N, 3°W). The most frequent precipitation features can be related to radar artifacts near the coast. These include the range rings from the Druim a'Starraig radar in the Hebrides; the lobes present offshore from the Hill of Dudwick radar; and the Castor Bay, Hameldon Hill, and Predannack radar sites. There is also increased occurrence of features from 100 to $1000 \, \mathrm{km}^2$ in southeastern Ireland likely related to artifacts from the Shannon radar.

The abovementioned regions of complex topography are also the areas where precipitation feature sizes of 1000–$10\,000 \, \mathrm{km}^2$ are more likely to occur (Fig. 9c), with up to $400 \, \mathrm{h \, yr^{-1}}$ (4.6%) over Wales and the west coast of Scotland compared to an average value of $130.8 \, \mathrm{h \, yr^{-1}}$ (1.5%) across the domain. Precipitation features in this area also occur more frequently from the Lake District through the Peak District, which runs through northwestern England. There is also a local maximum ($>240 \, \mathrm{h \, yr^{-1}}$, 2.7%) in Cornwall compared to the rest of Great Britain and Ireland. Features of this size are generally more likely to occur in Northern Ireland and near the Shannon radar compared to the rest of the domain, but because of the large areas of poor coverage in Ireland, this is relatively uncertain compared to results from the United Kingdom.

The effects of topography on the occurrence of precipitation features appear to decline as the feature sizes exceed $10\,000 \, \mathrm{km}^2$ (Fig. 9d), and are even less prevalent for feature sizes exceeding $100\,000 \, \mathrm{km}^2$. Even though only 2.6% of all precipitation features exceed $10\,000 \, \mathrm{km}^2$ and only 0.38% exceed $100\,000 \, \mathrm{km}^2$, these two size bins occur more frequently than the smaller bins. Because of their larger areas, larger precipitation features have longer residence times, which ultimately enhances their occurrence at any given grid point. Precipitation features with sizes of $10\,000$–$100\,000 \, \mathrm{km}^2$ (Fig. 9e) are more prevalent from Scotland to Northern Ireland and in the Peak District and Wales, and are particularly frequent over the west coast of Scotland with frequencies locally exceeding $700 \, \mathrm{h \, yr^{-1}}$ (8%). On average, there are $267 \, \mathrm{h \, yr^{-1}}$ (3%) of precipitation features with sizes of $10\,000$–$100\,000 \, \mathrm{km}^2$ and $270 \, \mathrm{h \, yr^{-1}}$ (3%) of precipitation features with sizes exceeding $100\,000 \, \mathrm{km}^2$. Edge effects are also apparent as the occurrence of larger features declines toward the boundary of the radar observation extent.

Although there are numerous radar artifacts contained in the calculation of the frequencies of occurrence of different size bins, many of these issues are mitigated by analyzing the contribution of each size bin to the total annual precipitation (Fig. 10). As similar artifacts are also present in the radar-derived precipitation total (cf. Figs. 3b and 10), dividing by this total
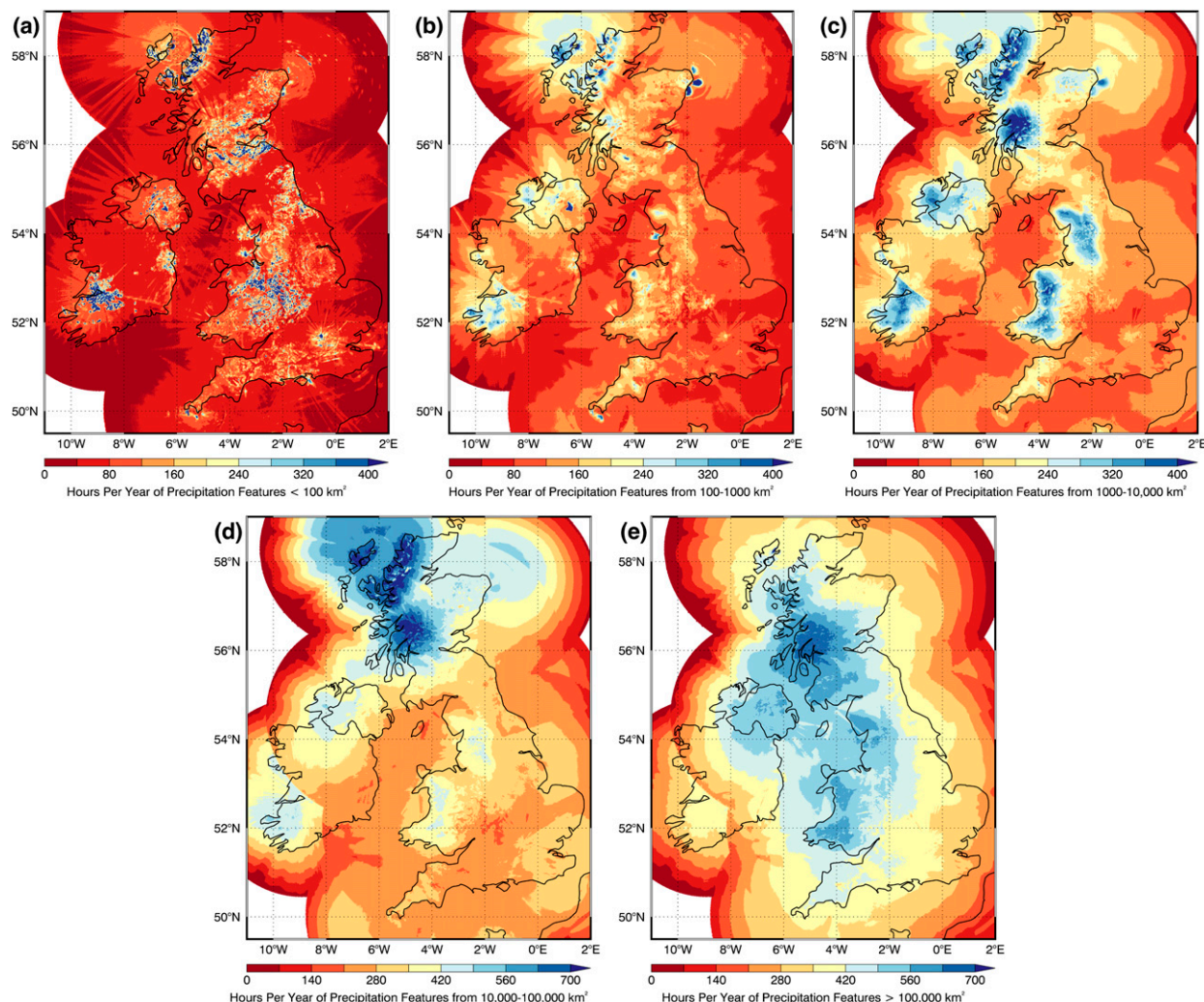
FIG. 9. Hours per year of precipitation feature occurrence for different area bins: (a) less than 100, (b) 100–1000, (c) 1000–10 000, (d) 10 000–100 000, and (e) exceeding 100 000 km². Note that scales vary.

cancels the majority of the errors. Small-scale features of less than 100 km² (Fig. 10a) contribute on average 3.7% to the total annual precipitation, with a consistently uniform pattern across much of Great Britain. There are occasional streaks of higher precipitation contribution, which can most likely be related to individual small-scale convective storms. The next larger size bin (Fig. 10b, 100–1000 km²) contributes around 10.3% of the total annual precipitation, varying from up to 16% on the west coast of Ireland to less than 6% over most of England. Features with an area of 1000–10 000 km² (Fig. 10c) contribute an average of 17% to the annual total of precipitation, with higher values on the west coast of Ireland and the west and east coasts of England. Areas of complex topography in Wales, Cornwall, and northwestern England also exhibit relatively high values, which could be related to the fact that

precipitation feature areas of this magnitude are roughly the same area as the orographic features themselves.

As precipitation feature sizes increase beyond 10 000 km², the fractional precipitation contribution increases greatly. Precipitation features ranging from 10 000 to 100 000 km² (Fig. 10d) contribute 34.9% of the annual total of precipitation, with features exceeding 100 000 km² (Fig. 10e) contributing 34.3% of all precipitation. There is a more uniform spatial distribution of the contribution for these two bins, and the patterns are inversely related, as the regions with the largest contributions in the bin from 10 000 to 100 000 km² are the regions with the smallest contribution in the bin exceeding 100 000 km², most likely due to precipitation features extending outside the boundaries of the radar composite. The largest features are only detectable in the center of the domain and then drop off toward the edges where they will fall more
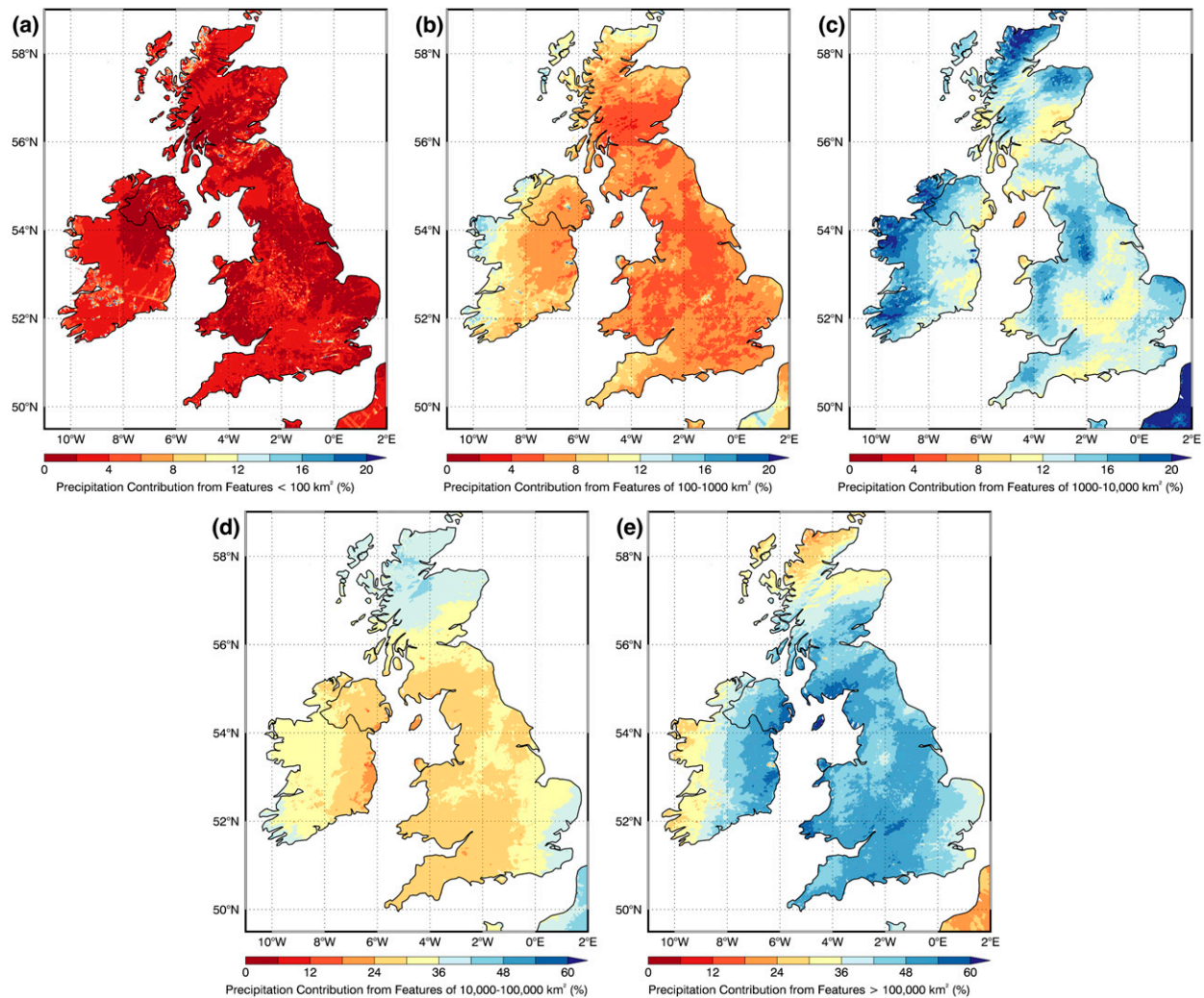
FIG. 10. Contribution to the annual total precipitation (%) from precipitation features of different area bins: (a) less than 100, (b) 100–1000, (c) 1000–10 000, (d) 10 000–100 000, and (e) exceeding 100 000 km². Note that scales vary.

within the 10 000–100 000 km² size bin. The largest contribution of precipitation from features exceeding 100 000 km² is found over the Isle of Man in the center of the Irish Sea, although small-scale storms over this island may occasionally go undetected due to its large distance from the nearest radar.

7. Characterization of Great Britain and Ireland banded precipitation

The two-dimensional shape of a precipitation feature as on a radar mosaic gives some clues to the physical mechanism behind the feature and the environment in which it developed. For example, isolated convective storms on a summer afternoon tend to initiate as small cellular shapes before possibly developing into mesoscale convective systems, even though these are rare

across the United Kingdom (Lewis and Gray 2010). Similarly, convection developing over elevated terrain can remain anchored in place or propagate downwind, forming linear bands of precipitation that can potentially lead to local extremes in precipitation accumulation. These bands have been identified over the United Kingdom, particularly in areas of complex topography (e.g., Golding et al. 2005; Barrett et al. 2015, 2016; Warren et al. 2014) and over the English Channel (Norris et al. 2013, and references therein).

Recall the definitions of the banded classifications given in section 2 for precipitation bands, mesoscale precipitation bands and mesoscale convective precipitation bands. The occurrence of banded precipitation (Fig. 11a) shows a similar pattern to the precipitation occurrence maps (cf. Figs. 3 and 11a). Primarily, there are more hours per year of banded
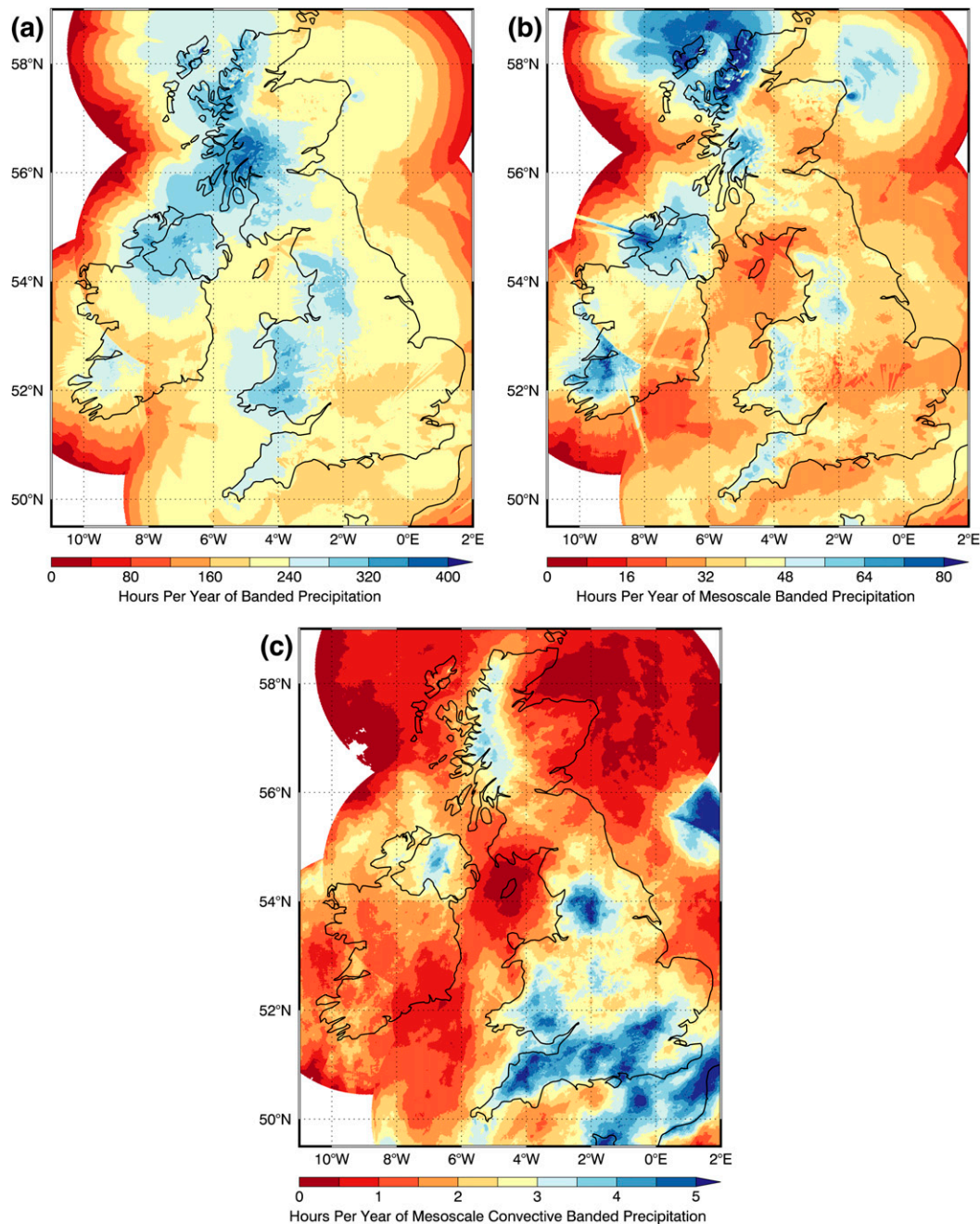
FIG. 11. Hours per year of occurrence of different types of precipitation features as defined in this study: (a) banded precipitation features, (b) mesoscale banded precipitation features, and (c) mesoscale convective banded precipitation features. Note that scales vary.

precipitation over areas of complex topography: the west coast of Scotland and Northern Ireland. On average, there are 172 h yr^{-1} (2%) of banded precipitation occurrence over the radar coverage area.

When limited to only mesoscale bands (Fig. 11b), the pattern does not change substantially, with the highest areas of occurrence located similarly. Areas such as the

north coast of Cornwall (covering 50°–51°N, 4°–6°W), along with Wales and the Peak District, are still local maxima, with individual features more clearly visible. There are also numerous radar artifacts that appear as anomalously high frequencies of mesoscale banded features. These spurs originate from the Castor Bay radar in Northern Ireland, the Shannon radar in

Ireland, and the Druim a'Starraig radar in Scotland. The occurrence of mesoscale banded precipitation features is only around 16% of the occurrence of all banded precipitation and on average occurs for $31.7 \, h \, yr^{-1}$ (0.4%).

The pattern of mesoscale convective banded features (Fig. 11c) clearly differs from the other banded precipitation occurrence maps. These features occur over the west coast of Scotland for $3–4 \, h \, yr^{-1}$, but have a strong maximum over the Peak District near 54°N, 2°W of over $5 \, h \, yr^{-1}$. Similar maxima are found in southern Wales and in an area extending from Cornwall to London and over the English Channel, agreeing with previous studies that have identified convection occurring more in the south of England and over the English Channel. On average, mesoscale convective banded precipitation features occur for $1.8 \, h \, yr^{-1}$ across the radar coverage area.

The contribution to the total precipitation by bands shows a fairly uniform north–south gradient from values as low as 20% over Ireland to more than 28% over southeastern England (Fig. 12a). Banded precipitation features contribute 26% of all precipitation across Great Britain and Ireland. By contrast, mesoscale banded precipitation features contribute much less to the total precipitation, with maxima rarely exceeding 5% over areas in Cornwall and the southeastern England coast (Fig. 12b). Areas with the least precipitation contribution from mesoscale bands are most of Scotland from 56° to 57°N and the Lake District and northern Wales, where less than 2% of the total precipitation is banded. In Ireland, there is a noticeable streak of misidentified precipitation band caused by a spurious spoke originating from the Castor Bay radar. On average, 4.4% of all precipitation over Great Britain and Ireland is contributed by mesoscale precipitation bands. Finally, mesoscale convective bands contribute 1%–2% of the annual precipitation in southern England from Cornwall through London and in areas near the Peak District (Fig. 12c). There are small maxima exceeding 2% that may be attributed to single storms that caused heavy flooding, including an area to the north of London. On average across the domain, mesoscale convective precipitation bands contribute 0.7% of the total annual precipitation.

The seasonal variation in banded precipitation is shown in Fig. 13. Precipitation bands occur more during SON and DJF than during MAM and JJA, possibly due to sharp precipitation lines originating along trailing cold fronts of strong midlatitude cyclones. The spatial pattern of occurrence in each season is very similar to the annual pattern of occurrence (cf. Figs. 11a and 13). However, bands are slightly more likely to occur over the English Channel during DJF relative to other months, reflecting the influence of snowbands that form there (Norris et al. 2013).

8. Comparison to previous studies

The feature-based methodology for precipitation analysis used herein was also used in Fairman et al. (2016) to determine the climatology of banded precipitation across the contiguous United States. One difference between our United States and Great Britain and Ireland climatologies was the prescribed minimum feature size, which over the United States was larger ($500 \, km^2$) compared to that used over Great Britain and Ireland ($100 \, km^2$). Another difference between these two studies was the minimum threshold for feature detection, which was due to the different radar networks present in each country. Over the United States, a 20-dBZ threshold was used for precipitation features. A 20-dBZ threshold corresponds to a $0.6 \, mm \, h^{-1}$ precipitation rate for Great Britain and Ireland, whereas the present study used a $0.0 \, mm \, h^{-1}$ precipitation rate. However, Fairman et al. (2016) found little difference among different reflectivity thresholds in 5-dBZ intervals in detecting precipitation bands, so the climatologies of precipitation from the two studies can be compared.

The precipitation feature cumulative frequency distributions [Fig. 3 in Fairman et al. (2016) and Fig. 5 in the present study] of different feature characteristics for the two different study areas are broadly similar, with a lognormal distribution of precipitation feature area and major axis length present in both studies. However, the diurnal patterns of precipitation feature characteristics [Fig. 4 in Fairman et al. (2016) and Fig. 6 in the present study] differ greatly. The diurnal pattern associated with convective storm growth that is attributed to afternoon convection in the United States is not present at all in Great Britain and Ireland [cf. Fig. 4a in Fairman et al. (2016) and Fig. 6a in the present study]. Over Great Britain and Ireland, the total precipitation area is largest during October– March, which can be attributed to the storm track traversing over the area. Over the United States, however, the total precipitation area is largest during summer when convection is present.

If we apply the minimum feature size of $500 \, km^2$ used over the United States in Fairman et al. (2016) to Great Britain and Ireland precipitation features, 12.2% of Great Britain and Ireland precipitation features would be banded compared to 14.8% in the United States. This difference is statistically significant by Student's t test at a 99.9% level. Seasonally, the patterns of banded
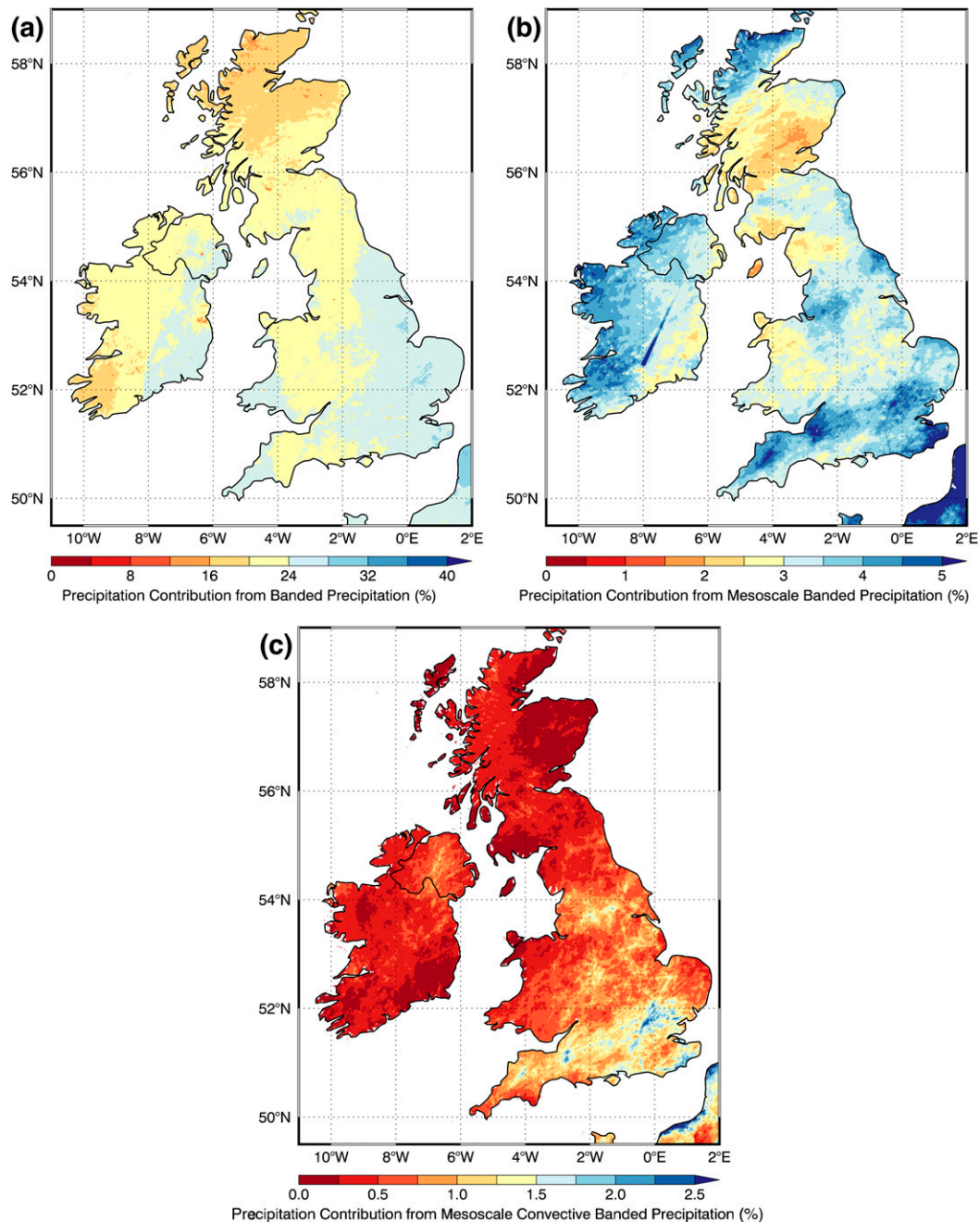
FIG. 12. Contribution to the annual precipitation total (%) from the different types of precipitation features defined in this study: (a) banded precipitation features, (b) mesoscale banded precipitation features, and (c) mesoscale convective banded precipitation features. Note that scales vary.

precipitation in the United States [Fig. 9 of Fairman et al. (2016)] show fewer occurrences of precipitation bands during JJA, similar to that over the United Kingdom (Fig. 13c). However, localized band hotspots in the United States due to frequent lake-effect snow generally do not exist in Great Britain and Ireland. The patterns of Great Britain and Ireland banded

precipitation also do not appreciably change from season to season, with the most frequent banding tied to topographic features. In contrast, the maximum of banded activity in the eastern United States undergoes a latitudinal cycle with season: moving equatorward during the winter and poleward during the summer.
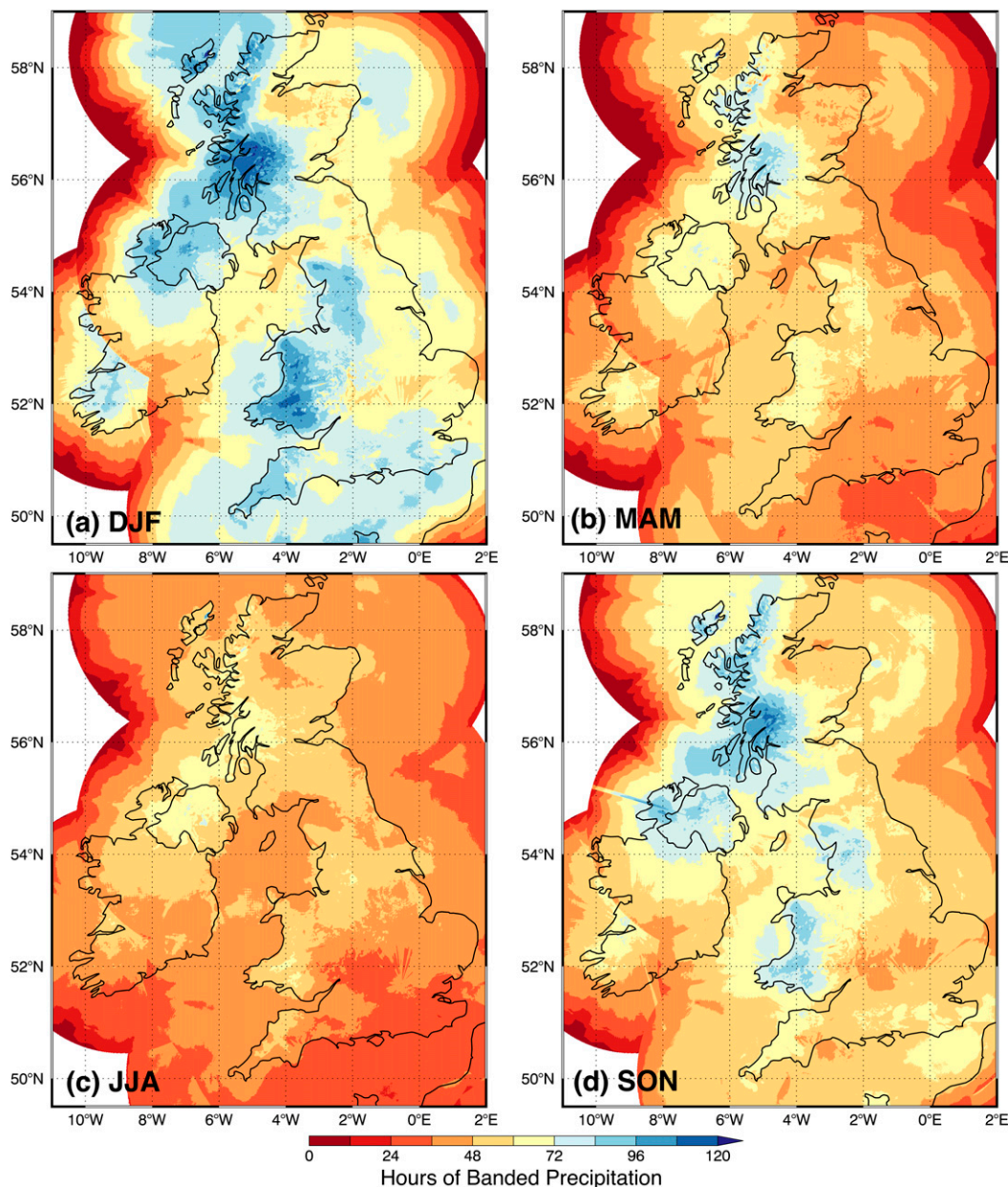
FIG. 13. Annual cycle of banded precipitation occurrence. Annual average hours per year of banded precipitation occurrence during (a) DJF, (b) MAM, (c) JJA, and (d) SON.

Figure 14 shows banded precipitation percentage by occurrence for Great Britain and Ireland and is directly comparable to Fig. 8 of Fairman et al. (2016) for the United States. Whereas over 30% of precipitation east of the Mississippi is banded in most of the continental United States [cf. Fig. 8 in Fairman et al. (2016) and Fig. 14 in the present study], only 12%–20% of precipitation in Great Britain and Ireland (Fig. 14) is banded. The banded precipitation percentage of Great Britain and Ireland is therefore the most comparable to

that found in the western United States and is particularly similar to that found in Florida.

Rickenbach et al. (2015) found that 70%–90% of precipitation across the southeastern United States originated from mesoscale precipitation features. These mesoscale precipitation features were separated from ''isolated'' precipitation features by using a major axis length threshold of 100 km. Their results broadly agree with the fractional contribution of larger precipitating systems across Great Britain and Ireland found in this
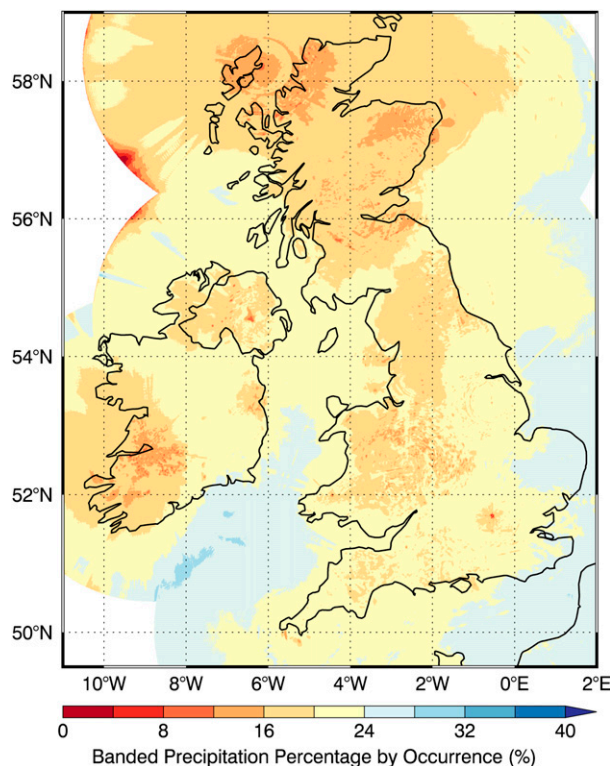
FIG. 14. Banded precipitation percentage by occurrence, comparable to Fig. 8 of Fairman et al. (2016).

study, where an average of nearly 70% of precipitation originates from precipitation features that equal or exceed $10\,000\,km^2$ in area, even with the differences in thresholding between major axis length and area.

Although TRMM climatologies of precipitation only cover areas from 37.5°S to 37.5°N, they can also be compared to Great Britain and Ireland precipitation to give a context as to how Great Britain and Ireland midlatitude precipitation compares to the global distribution of precipitation in the tropics and subtropics. Yang and Nesbitt (2014) found that 73% of global precipitation over land occurs from precipitation intensities of less than $5\,mm\,h^{-1}$. Over Great Britain and Ireland, 97.3% of all precipitation occurrences are from precipitation intensities less than $5\,mm\,h^{-1}$, which indicates that light rain contributes a larger fraction of annual rainfall in Great Britain and Ireland than it does in the tropics and subtropics. The contribution to the total precipitation from precipitation intensities less than $5\,mm\,h^{-1}$ from TRMM is around 40% over the tropical areas, but 83.6% over Great Britain and Ireland. Long-lived light precipitation therefore appears to contribute much more to precipitation across Great Britain and Ireland. However, light rainfall may go undetected by the TRMM Precipitation Radar more often than by the

ground-based radars in our composite, as noted by Yang and Nesbitt (2014).

9. Conclusions

This study is the first to quantify the size (by amount of area covered), shape (by fitted ellipse), and intensity of precipitating features across Great Britain and Ireland. A regional radar-derived precipitation mosaic is used to identify 54 811 747 precipitating features over $100\,km^2$ in area from 2006 to 2015. At any given time over the radar coverage area, there are on average 54 unique features, with a median feature size of $249\,km^2$, median axis length of 29.2 km, and median aspect ratio of 2.02:1. The median mean feature precipitation rate is $0.49\,mm\,h^{-1}$ with a median maximum precipitation rate within the feature of $2.4\,mm\,h^{-1}$. The median precipitation feature size is equivalent to that of a circle with a diameter of 18 km and has an intensity that could be classified on average as light rain.

On average, a precipitation feature is larger during the winter than the summer. A strong diurnal signature exists in precipitation feature intensity during the summer, with both the mean precipitation rate and maximum precipitation rate increasing throughout the afternoon hours. The maximum feature precipitation rate is highest during July at 1500 UTC, whereas the mean feature precipitation rate is highest during December. Although there is little diurnal variation in many feature characteristics outside of the mean and maximum precipitation rates during summer, there is a strong seasonal difference in the area covered by precipitation, with the winter having around 3 times the area covered by precipitation compared to the summer.

Mesoscale precipitation features less than $10\,000\,km^2$ in area are most often found in areas of topographic variation such as Wales, the Lake District into the Peak District, and the west coast of Scotland. These mesoscale features are also more likely to occur in Ireland. However, large-scale precipitation dominates, with precipitation features of greater than $10\,000\,km^2$ contributing nearly 70% of the total precipitation across the domain. Precipitation rates between 0 and $1\,mm\,h^{-1}$ are most frequent. In contrast, the largest contribution to the annual precipitation total comes from precipitation intensities between 1 and $5\,mm\,h^{-1}$, with 83.6% of precipitation originating from all precipitation rates less than $5\,mm\,h^{-1}$.

Three different classes of banded features were defined based upon the characteristics of the individual precipitation features: banded features, with an aspect ratio greater than or equal to 3:1 and a major axis greater than or equal to 100 km; mesoscale banded features,

with an aspect ratio exceeding 3:1 and axis length greater than or equal to 100 km and area not exceeding $10\,000\,km^2$; and mesoscale convective banded features, which have all of the characteristics of mesoscale banded features and additionally have at least $100\,km^2$ of area with a precipitation rate exceeding $10\,mm\,h^{-1}$. Of all identified features, 3.2% are banded features, 2.5% are mesoscale banded features, and 0.09% are mesoscale convective banded features. This classification indicates that long-lived convective precipitation bands are uncommon within the feature database. When comparing precipitation bands in Great Britain and Ireland to the contiguous United States, the percentage of banded precipitation over Great Britain and Ireland is similar to that found in Florida, with the Midwest showing a higher percentage of banded precipitation and the western United States a lower percentage of banded precipitation.

This observational analysis is based upon a decade-long dataset using techniques that can be easily compared with output from numerical models. Comparison of the distribution of precipitation feature characteristics from a numerical model to Great Britain and Ireland radar mosaic may help to identify model strengths and weaknesses in the representation of the morphology of precipitating systems.

APPENDIX

Description of the Feature Detection Algorithm

To determine major and minor axis lengths of the individual precipitation features, a mass-density method of ellipse fitting was used. This method was derived from the Fit_Ellipse program of the Coyote IDL Library (http://www.idlcoyote.com), with all analysis in this study being performed using IDL 8.1. The mass-fitting method operates as follows. All X/Y locations of each pixel in the feature are calculated, and the center of mass is calculated. Positions in the region of interest relative to this center of mass are then calculated and totaled to calculate the mass distribution tensor. The eigenvalues of the mass distribution tensor determine the axes and orientation of a fitted ellipse.

REFERENCES

Antonescu, B., G. Vaughan, and D. M. Schultz, 2013: A five-year radar-based climatology of tropopause folds and deep convection over Wales, United Kingdom. *Mon. Wea. Rev.*, **141**, 1693–1707, doi:10.1175/MWR-D-12-00246.1.

Barrett, A. I., S. L. Gray, D. J. Kirshbaum, N. M. Roberts, D. M. Schultz, and J. G. Fairman Jr., 2015: Synoptic versus orographic control on stationary convective banding. *Quart. J. Roy. Meteor. Soc.*, **141**, 1101–1113, doi:10.1002/qj.2409.

——, ——, ——, ——, ——, and ——, 2016: The utility of convection-permitting ensembles for the prediction of stationary convective bands. *Mon. Wea. Rev.*, **144**, 1093–1114, doi:10.1175/MWR-D-15-0148.1.

Cecil, D. J., S. J. Goodman, D. J. Boccippio, E. J. Zipser, and S. W. Nesbitt, 2005: Three years of TRMM precipitation features. Part I: Radar, radiometric and lightning characteristics. *Mon. Wea. Rev.*, **133**, 543–566, doi:10.1175/MWR-2876.1.

Fairman, J. G., Jr., D. M. Schultz, D. J. Kirshbaum, S. L. Gray, and A. I. Barrett, 2015: A radar-based rainfall climatology of Great Britain and Ireland. *Weather*, **70**, 153–158, doi:10.1002/wea.2486.

——, ——, ——, ——, and ——, 2016: Climatology of banded precipitation over the contiguous United States. *Mon. Wea. Rev.*, **144**, 4553–4568, doi:10.1175/MWR-D-16-0015.1.

Georgiou, S., N. Gaussiat, and H. Lewis, 2011: Analysis of a scheme to dynamically model the orographic enhancement of precipitation in the UK. *IAHS Publ.*, **351**, 201–206.

Golding, B., P. Clark, and B. May, 2005: The Boscastle flood: Meteorological analysis of the conditions leading to flooding on 16 August 2004. *Weather*, **60**, 230–235, doi:10.1256/wea.71.05.

Harrison, D. L., R. W. Scovell, and M. Kitchen, 2009: High-resolution precipitation estimates for hydrological uses. *Proc. Inst. Civ. Eng.: Water Manage.*, **162**, 125–135, doi:10.1680/wama.2009.162.2.125.

——, K. Norman, C. Pierce, and N. Gaussiat, 2012: Radar products for hydrological applications in the UK. *Proc. Inst. Civ. Eng.: Water Manage.*, **165**, 89–103, doi:10.1680/wama.2012.165.2.89.

Hou, A. Y., and Coauthors, 2014: The Global Precipitation Measurement Mission. *Bull. Amer. Meteor. Soc.*, **95**, 701–722, doi:10.1175/BAMS-D-13-00164.1.

Jiang, H., C. Liu, and E. J. Zipser, 2011: A TRMM-based tropical cyclone cloud and precipitation feature database. *J. Appl. Meteor. Climatol.*, **50**, 1255–1274, doi:10.1175/2011JAMC2662.1.

Kirshbaum, D. J., F. Fabry, and Q. Cazenave, 2016: The Mississippi Valley convection minimum on summer afternoons: Observations and numerical simulations. *Mon. Wea. Rev.*, **144**, 263–272, doi:10.1175/MWR-D-15-0238.1.

Kitchen, M., and A. Illingworth, 2011: From observations to forecasts—Part 13: The UK weather radar network—Past, present and future. *Weather*, **66**, 291–297, doi:10.1002/wea.861.

——, R. Brown, and A. G. Davies, 1994: Real-time correction of weather radar data for the effects of bright band, range and orographic growth in widespread precipitation. *Quart. J. Roy. Meteor. Soc.*, **120**, 1231–1254, doi:10.1002/qj.49712051906.

Kummerow, C., W. Barnes, T. Kozu, J. Shiue, and J. Simpson, 1998: The Tropical Rainfall Measuring Mission (TRMM) sensor package. *J. Atmos. Oceanic Technol.*, **15**, 809–817, doi:10.1175/1520-0426(1998)015<0809:TTRMMT>2.0.CO;2.

Leary, C. A., and R. A. Houze Jr., 1979: Melting and evaporation of hydrometeors in precipitation from the anvil clouds of deep tropical convection. *J. Atmos. Sci.*, **36**, 669–679, doi:10.1175/1520-0469(1979)036<0669:MAEOHI>2.0.CO;2.

Lewis, H. W., and D. L. Harrison, 2007: Assessment of radar data quality in upland catchments. *Meteor. Appl.*, **14**, 441–454, doi:10.1002/met.43.

Lewis, M. W., and S. L. Gray, 2010: Categorisation of synoptic environments associated with mesoscale convective systems over the UK. *Atmos. Res.*, **97**, 194–213, doi:10.1016/j.atmosres.2010.04.001.

Liu, C., and E. J. Zipser, 2013: Regional variation of morphology of organized convection in the tropics and subtropics. *J. Geophys. Res. Atmos.*, **118**, 453–466, doi:10.1029/2012JD018409.

——, ——, D. J. Cecil, S. W. Nesbitt, and S. Sherwood, 2008: A cloud and precipitation feature database from nine years of TRMM observations. *J. Appl. Meteor. Climatol.*, **47**, 2712–2728, doi:10.1175/2008JAMC1890.1.

Maddox, R. A., 1980: Mesoscale convective complexes. *Bull. Amer. Meteor. Soc.*, **61**, 1374–1387, doi:10.1175/1520-0477(1980)061<1374:MCC>2.0.CO;2.

Marshall, J. S., and W. K. M. Palmer, 1948: The distributions of raindrops with size. *J. Meteor.*, **5**, 165–166, doi:10.1175/1520-0469(1948)005<0165:TDORWS>2.0.CO;2.

——, W. Hitschfeld, and K. L. S. Gunn, 1955: Advances in radar weather. *Advances in Geophysics*, Vol. 2, Academic Press, 1–56, doi:10.1016/S0065-2687(08)60310-6.

Met Office, 1997: *Forecasters' Reference Book*. Met Office, 176 pp. [Available online at https://digital.nmla.metoffice.gov.uk/file/sdb%3AdigitalFile%7C103a272a-2f1e-4837-a954-b1a5b53ae84a/.]

——, 2003: Met Office rain radar data from the NIMROD system. NCAS British Atmospheric Data Centre, accessed 4 January 2016. [Available online at http://catalogue.ceda.ac.uk/uuid/82adec1f896af6169112d09cc1174499.]

——, 2009: Radar. National Meteorological Library and Archive Fact Sheet 15, 22 pp. [Available online at http://www.metoffice.gov.uk/learning/library/publications/factsheets.]

Nesbitt, S. W., E. J. Zipser, and D. J. Cecil, 2000: A census of precipitation features in the Tropics using TRMM: Radar, ice scattering, and lighting observations. *J. Climate*, **13**, 4087–4016, doi:10.1175/1520-0442(2000)013<4087:ACOPFI>2.0.CO;2.

——, R. Cifelli, and S. A. Rutledge, 2006: Storm morphology and rainfall characteristics of TRMM precipitation features. *Mon. Wea. Rev.*, **134**, 2702–2721, doi:10.1175/MWR3200.1.

Norris, J., G. Vaughan, and D. M. Schultz, 2013: Snowbands over the English Channel and Irish Sea during cold-air outbreaks. *Quart. J. Roy. Meteor. Soc.*, **139**, 1747–1761, doi:10.1002/qj.2079.

Rapp, A. D., A. G. Peterson, O. W. Frauenfeld, S. M. Quiring, and E. B. Roark, 2014: Climatology of storm characteristics in Costa Rica using the TRMM Precipitation Radar. *J. Hydrometeor.*, **15**, 2615–2633, doi:10.1175/JHM-D-13-0174.1.

Rasmussen, K. L., M. M. Chaplin, M. D. Zuluaga, and R. A. Houze Jr., 2016: Contribution of extreme convective storms to rainfall in South America. *J. Hydrometeor.*, **17**, 353–367, doi:10.1175/JHM-D-15-0067.1.

Rickenbach, T. M., R. Nieto-Ferreria, C. Zarzar, and B. Nelson, 2015: A seasonal and diurnal climatology of precipitation organization in the southeastern United States. *Quart. J. Roy. Meteor. Soc.*, **141**, 1938–1956, doi:10.1002/qj.2500.

Skofronick-Jackson, G., and Coauthors, 2017: The Global Precipitation Measurement (GPM) Mission for Science and Society. *Bull. Amer. Meteor. Soc.*, doi:10.1175/BAMS-D-15-00306.1, in press.

Smalley, M., and T. L'Ecuyer, 2015: A global assessment of the spatial distribution of precipitation occurrence. *J. Appl. Meteor. Climatol.*, **54**, 2179–2197, doi:10.1175/JAMC-D-15-0019.1.

Warren, R. A., D. J. Kirshbaum, R. S. Plant, and H. W. Lean, 2014: A 'Boscastle-type' quasi-stationary convective system over the UK southwest peninsula. *Quart. J. Roy. Meteor. Soc.*, **140**, 240–257, doi:10.1002/qj.2124.

Woollings, T., C. Czuchnicki, and C. Franzke, 2014: Twentieth century North Atlantic jet variability. *Quart. J. Roy. Meteor. Soc.*, **140**, 783–791, doi:10.1002/qj.2197.

Xu, W., R. F. Adler, and N.-Y. Wang, 2014: Combining satellite infrared and lightning information to estimate warm-season convective and stratiform rainfall. *J. Appl. Meteor. Climatol.*, **53**, 180–199, doi:10.1175/JAMC-D-13-069.1.

——, and S. A. Rutledge, 2015: Morphology, intensity, and rainfall production of MJO convection: Observations from DYNAMO shipborne radar and TRMM. *J. Atmos. Sci.*, **72**, 623–640, doi:10.1175/JAS-D-14-0130.1.

Yang, S., and S. W. Nesbitt, 2014: Statistical properties of precipitation as observed by the TRMM Precipitation Radar. *Geophys. Res. Lett.*, **41**, 5636–5643, doi:10.1002/2014GL060683.

Zhang, J., and Coauthors, 2011: National Mosaic and Multi-Sensor QPE (NMQ) system: Description, results, and future plans. *Bull. Amer. Meteor. Soc.*, **92**, 1321–1338, doi:10.1175/2011BAMS-D-11-00047.1.

Zipser, E. J., C. Liu, D. J. Cecil, S. W. Nesbitt, and D. P. Yorty, 2006: Where are the most intense thunderstorms on Earth? *Bull. Amer. Meteor. Soc.*, **87**, 1057–1071, doi:10.1175/BAMS-87-8-1057.